Crackling Dynamics in the Mechanical Response of Knitted Fabrics

Samuel Poincloux,[1,*] Mokhtar Adda-Bedia,[2] and Frédéric Lechenault[1]
[1]Laboratoire de Physique Statistique, Ecole Normale Supérieure, PSL Research University, Sorbonne University, CNRS, F-75231 Paris, France
[2]Université de Lyon, Ecole Normale Supérieure de Lyon, Université Claude Bernard, CNRS, Laboratoire de Physique, F-69342 Lyon, France

(Received 21 March 2018; revised manuscript received 8 June 2018; published 30 July 2018)

Crackling noise, which occurs in a wide range of situations, is characterized by discrete events of various sizes, often correlated in the form of avalanches. We report experimental evidence that the mechanical response of a knitted fabric displays such broadly distributed events both in the force signal and in the deformation field, with statistics analogous to that of earthquakes or soft amorphous materials. A knit consists of a regular network of frictional contacts, linked by the elasticity of the yarn. When deformed, the fabric displays spatially extended avalanchelike yielding events resulting from collective interyarn contact slips. We measure the size distribution of these avalanches, at the stitch level from the analysis of nonelastic displacement fields and externally from force fluctuations. The two measurements yield consistent power law distributions reminiscent of those found in other avalanching systems. Our study shows that a knitted fabric is not only a thread-based metamaterial with highly sought after mechanical properties, but also an original, model system, with topologically protected structural order, where an intermittent, scale-invariant response emerges from minimal ingredients, and thus a significant landmark in the study of out-of-equilibrium universality.

DOI: 10.1103/PhysRevLett.121.058002

Crackling dynamics in a material mechanical response is currently intensively studied owing to its fundamental and industrial relevance and to the vast range of systems it encompasses. Indeed, examples of such a response is usually found in disordered physical systems like granular materials [1–3], foams [4], metallic glasses [5,6], seismic regions [7], or front propagation in heterogeneous media [8,9] but is also documented in structurally ordered situations [10–12]. In the case of soft amorphous materials, though the origin of elasticity and plasticity and their typical length scales [13] largely differ from one system to another, a common framework has been established to investigate and predict the avalanche features [14–16].

This work aims at demonstrating that, despite their fundamentally ordered nature, knitted fabrics can also be studied within this framework. A knit is made of an elastic yarn, morphed into a 2D surface by imposing a topological, periodic pattern of self-crossing points, resulting in a network of so-called stitches [Fig. 1(a)]. Stitches deform elastically through bending of the yarn, but friction at the crossing points adds an uncertainty to the contact forces, inducing irreversible stick-slip activity. Those events propagate in the stitch network, generating avalanches and producing plastic events in the mechanical response. In this study, we use tools borrowed from the study of soft amorphous materials to characterize, externally and internally, the avalanches in this system and illustrate why it provides a handy tool to make progress in this field.

Experiments.—We perform a tensile test on a model fabric, knitted out of a nylon monofilament of diameter 150 μm (Stroft® GTM), and record its stitch displacement fields and global mechanical response. The sample is crafted using a single-bed knitting machine and is composed of 83×83 stitches with an average lateral and longitudinal size of, respectively, 3.9 and 2.8 mm. It is then clamped on its upper and lower rows, preventing lateral displacement of the corresponding stitches. The tensile test consists on varying cyclically L, the elongation of the fabric along the so-called wale direction, between $L_i = 215$ mm and $L_f = 234$ mm. The mechanical response is analyzed during the stretching phase on a shorter elongation range, between $L_m = 230$ mm and L_f. In this interval, the force needed to deform the fabric is recorded at a high acquisition frequency with an Instron® mounted with a 50 N load cell, and high-resolution pictures (7360×4912 pixels) of the sample are taken every $\Delta L = 0.2$ mm increase in elongation. To approach the quasistatic deformation limit in the interval $[L_m, L_f]$, we impose a constant pulling speed v of the dynamometer and set it at a small value ranging from 1 to 10 μm/s. To reduce the duration of the experiment, we fix $v = 0.5$ mm/s outside this measurement window. The imposed elongation L as a function of time is shown in Supplemental Fig. S1 [17], and Supplemental Table S1 [17] summarizes the parameters of all conducted tensile tests. Finally, a typical image of the fabric and the recorded force during one measurement window are shown in Fig. 1.

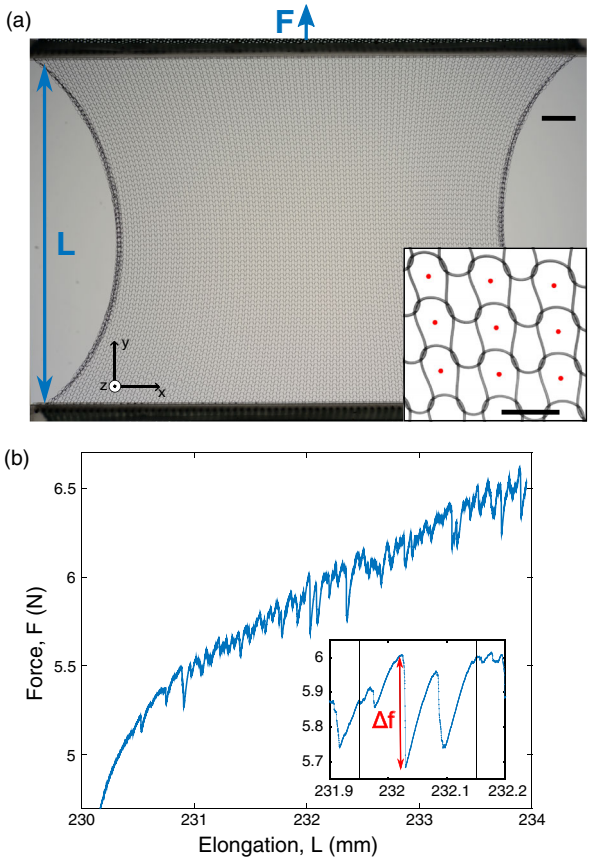

FIG. 1. Experimental system and typical force response. (a) A knitted fabric is stretched uniaxially while its mechanical response is recorded and the position of the stitches is tracked through digital image processing, with a precision of approximately 10 μm. Typical picture of the knit; the stretching direction is materialized by the arrow associated to the force F, while L denotes its elongation. The scale bar is 25 mm long. Inset: Enlargement over a few stitches tagged by a red dot indicating their position defined as their geometric center. Here the scale bar is 4 mm long. (b) Typical mechanical response of the fabric while stretched between $L_m = 230$ mm and $L_f = 234$ mm at a constant speed of $v = 5$ μm/s. Stick-slip events at the contact points generate an intermittent signal, typical of crackling dynamics. Inset: Enlargement over a small interval, the definition of Δf is emphasized, and the two vertical lines distant by $\Delta L = 0.2$ mm point to elongations at which two successive pictures of the fabric are taken.

Estimation of avalanche size.—Upon stretching, the force signal displays, around an average elastic response, typical force fluctuations indicative of avalanches. The fluctuations consist in linear regions, stiffer than the average response, interrupted by plastic events provoking abrupt drops. The height of the drops Δf can be measured and is expected to be correlated to the avalanche size. Furthermore, evidence of those avalanches is identified in the deformation field of the stitch network. Performing an external measurement associated with an internal one is crucial to characterize the events and to rule out other possible phenomena.

Digital image processing allows us to recover the position field of the stitch network, and its displacement field between two successive pictures $\vec{u}_{\mathrm{tot}}$ is computed. To emphasize its nonelastic component, the affine part $\vec{u}_{\mathrm{lin}}$ is removed. We name $\vec{u}$ the resulting nonaffine displacement field: $\vec{u} = \vec{u}_{\mathrm{tot}} - \vec{u}_{\mathrm{lin}} = u_x\vec{e}_x + u_y\vec{e}_y$; Supplemental Fig. S2 [17] illustrates such an operation. Figure 2(a) shows that the nonaffine displacement field appears highly heterogeneous, with abrupt spatial changes in the direction and size of $\vec{u}$ seemingly organized along diagonal lines. Those changes indicate that regions of the fabric are sliding against one another and are reminiscent of dislocation lines in crystals [18]. However, unlike the crystalline case, the connectivity of the network is locked, and sliding events remain small compared to the size of a unit cell. On that account, in order to characterize the features in $\vec{u}$, we use two invariants of the deformation tensor [19]: the vorticity $\omega = \{[(\partial u_y)/(\partial x)] - [(\partial u_x)/(\partial y)]\}$ and the deviatoric strain $\varepsilon_d = \sqrt{\{[(\partial u_x)/(\partial x)] - [(\partial u_y)/(\partial y)]\}^2 + \{[(\partial u_y)/(\partial x)] + [(\partial u_x)/(\partial y)]\}^2}$. The values of ω and ε_d associated to the displacement field depicted in Fig. 2(a) are displayed in, respectively, Figs. 2(b) and 2(c) [see Movie S1 in Supplemental Material [17] showing these fields for different ΔL along the curve $F(L)$ in Fig. 1(b)]. The boundaries between sliding regions of the knit are well captured by the two invariants ω and ε_d, which hence are good candidates to evaluate the size of the sliding events from the local measurements. In contrast, it is worth noticing that $\vec{\nabla}\cdot\vec{u}$ and the shear strain $[(\partial u_y)/(\partial x)] + [(\partial u_x)/(\partial y)]$ are always vanishingly small and show no significant variation in the vicinity of a sliding line (see Supplemental Fig. S3 [17]). The sign of ω allows us to discern two main event orientations: We define positive events as those featuring $\omega > 0$ and negative ones as those with $\omega < 0$. To retrieve an event size S_ω from the scalar fields ω, we detect the connected stitches with $|\omega|$ higher than a threshold value and then integrate $|\omega|$ over those stitches. A demonstration of this process is shown in Supplemental Fig. S4 [17]. The same operation is applied to measure the event size S_d from ε_d.

Finally, we have verified that the location and size of sliding events are robust against the use of the total vector field $\vec{u}_{\mathrm{tot}}$, instead of $\vec{u}$, for the definition of ω and ϵ_d. This is mainly due to the fact that, even though a heterogeneous underlying loading is applied to the fabric, the spatial variations of $\vec{u}_{\mathrm{lin}}$ are small compared to those due to plastic events.

Distribution of avalanche size.—We now have a tool to measure the size of "quakelike" events, from an external perspective with the force drops Δf but also internally using two different means: high vorticity regions S_ω and high deviatoric strain regions S_d. The protocol, and especially ΔL, is chosen such that the interval between

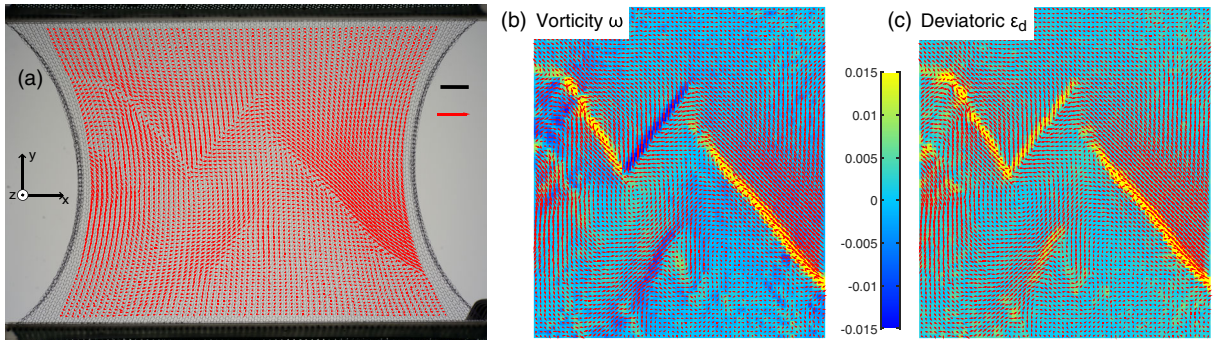

FIG. 2. Local detection of slip events. (a) Displacement field corresponding to the inset in Fig. 1(b). Each stitch is tagged by its nonaffine displacement $\vec{u}$, portrayed by red arrows magnified by a factor of 35. Black scale bar (position), 25 mm; red scale bar (displacement), 0.6 mm. (b) Vorticity ω and (c) deviatoric strain ε_d of the displacement field in the stitch network. Each arrow of the displacement field is associated to a single stitch.

pictures is much longer than the duration of an event; hence, each image is not correlated to the previous one, and each cycle can be seen as another, statistically independent trial. In that way, we can build up statistics to characterize the probability distribution of event size. Figure 3(a) shows this distribution for Δf, while Fig. 3(b) shows the ones for S_ω and S_d. The three distributions exhibit a power law decay with exponents of -1.50 ± 0.03 for Δf, -1.61 ± 0.03 for S_d, and -1.51 ± 0.05 for S_ω. Those power law distributions are characteristic of avalanching phenomena [5,6,8], and the exponents we find are consistent with the prediction $-3/2$ of mean-field models [15] for soft amorphous solids. However, the universality of this exponent is still debated [3,16,20]. These scaling laws are robust upon varying the threshold value of $|\omega|$ and ε_d for the event detection (Supplemental Fig. S5), the loading speed (Supplemental Fig. S6 for Δf and Fig. S7 for S_ω and S_d), or the stretching range (Supplemental Fig. S8) [17]. Internal and external measurements of event size have noticeably similar distribution, so one should probe if they are indeed two aspects of the same avalanches [21,22]. Thus, for each interval between two images, we sum S_ω and S_d over all the events detected within, giving, respectively, ΣS_ω and ΣS_d, and compare them to the sum of Δf, named $\Sigma \Delta f$, measured during the same interval. The resulting scatter plot [Fig. 3(a), inset] shows a clear linear tendency, which establishes a statistical correspondence between internal and external events. The slope $E_p = 0.12$ N allows us to extract an avalanche parameter relating plastic deformation and force drops. Besides, comparing ΣS_ω and ΣS_d [Fig. 3(b), inset] reveals proportionality with a coefficient close to 1. This suggests that, in this system, the sliding events are also characterized by a strong correlation between the deviatoric strain and the vorticity of the displacement field, as retrieved theoretically below.

Avalanche propagation.—Though it does not flow, the system at hand is reminiscent of soft amorphous solids which are commonly described using elastoplastic models [23]. These approaches assume the material as an elastic

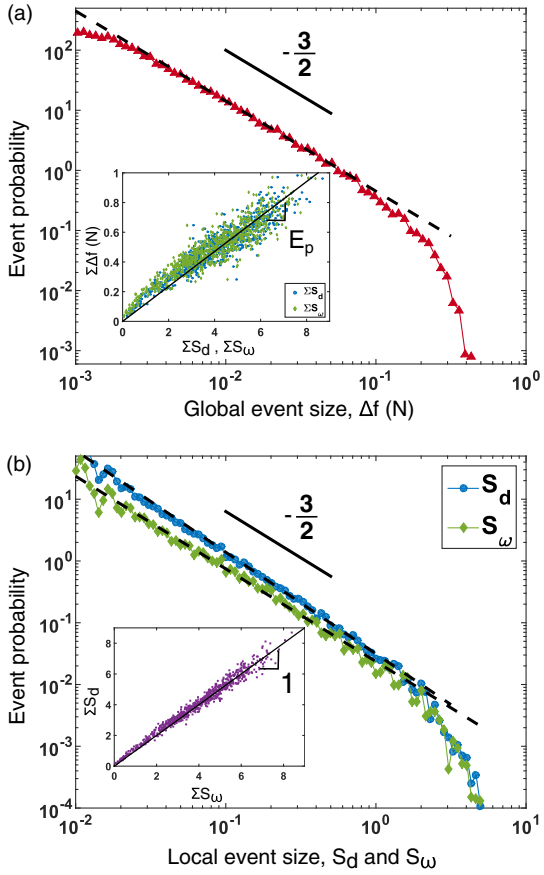

FIG. 3. Event size distribution measured from external and internal quantities. (a) Probability distribution of global event size measurement Δf. The dotted line is the best linear fit with a slope of -1.50 ± 0.03. Inset: For each interval between two images, the sum of event sizes measured externally is compared to the sum of events measured internally. (b) Probability distribution of local event size measurements from vorticity S_ω and deviatoric strain S_d of the displacement field. Dotted lines are the best linear fit with a slope of -1.51 ± 0.05 and -1.61 ± 0.03 for, respectively, S_ω and S_d. Inset: Comparison between the sum of S_ω and the sum of S_d for each interval. The loading speed for the data shown in this figure is $v = 5$ μm/s. The uncertainty in the exponents is evaluated from the standard error and a 95% confidence interval.

matrix with a plastic (or yield) limit and a distance to this limit distributed inhomogeneously in space [24,25]. While the stress is globally increased in the material, areas close to the plastic limit will yield first and induce a stress redistribution that may trigger other plastic events [26,27], resulting in propagating avalanches [14,28–30]. To test if a knitted fabric fits in this framework, we first analyze the nucleation and morphology of plastic events. The viewing of different images shows that the slip lines can actually intersect, although a V-shaped morphology seems to be the generic feature. To further assess this specific feature, we performed high-speed imagery of an avalanche (see Fig. S9 in Ref. [17]). It turns out that avalanches often start from a single, bulk stitch and then propagate from this particular site in all possible favored directions.

Now, let us study how plastic events are correlated in space [31]. Since high values of the vorticity in the nonaffine displacement field ω are a good signature of plastic events in our fabric, event spatial correlation can be evaluated with the following quantity:

$$C_{\omega}^{\pm}(\delta x,\delta y)=1+\frac{\langle\omega(x+\delta x,y+\delta y)-\omega(x,y)\rangle_{\pm}}{\langle\omega(x,y)\rangle_{\pm}}, \qquad (1)$$

where the average $\langle\rangle_{\pm}$ runs over all the stitches detected in a positive (+) or negative (−) event. C_{ω}^{+}, displayed in Fig. 4(a), presents a strong correlation in the direction $-(\pi/4)$, indicating that positive events propagate along the diagonal of the stitch network. For a negative event, the result is the same but with the direction $(\pi/4)$. To uncover the relation between the avalanche propagation and how the elastic matrix reacts to a local plastic event, we use a framework [32] which provides us with a continuous model of knit elasticity. Considering a homogeneous fabric, we locally impose a nonzero vorticity ω_0 and a deformation field $\varepsilon_{d_0}=\{[(\partial u_x)/(\partial x)]-[(\partial u_y)/(\partial y)]\}$ that is related to the deviatoric strain and allows us to account for the sign of this quantity. Those deformations are applied over a region of size d, with $\omega_0>0$ for a positive event and $\omega_0<0$ for a negative event, while $\varepsilon_{d_0}<0$ for both types of event. We then compute the resulting displacement field with a vanishing displacement far from the perturbation. In the stitch network, the vorticity and deviatoric strain have the following expressions in polar coordinates (r,θ): $\omega(r,\theta)=[(\varepsilon_{d_0}d^2)/(2r^2)]\sin 2\theta$ and $\varepsilon_d(r,\theta)=[(\omega_0 d^2)/(2r^2)]\sin 2\theta$, valid for $r\geq d$. More details on the elastic model and calculations can be found in Supplemental Material [17]. The resulting displacement field around a positive event is shown in Fig. 4(b), together with the angular variation of $\omega(r,\theta)$. The elastic response of the knit allows us to retrieve two properties of the measured events. First, the maxima of the vorticity and deviatoric fields are located along the same directions as those measured experimentally, irrespective of the event sign. Second, the elastic model gives $\omega(r,\theta)$ directly proportional to ε_{d_0}, along with $\varepsilon_d(r,\theta)$ proportional to ω_0, suggesting that, during event propagation, the vorticity and deviatoric are strongly correlated as evidenced experimentally [see the inset in Fig. 3(b)].

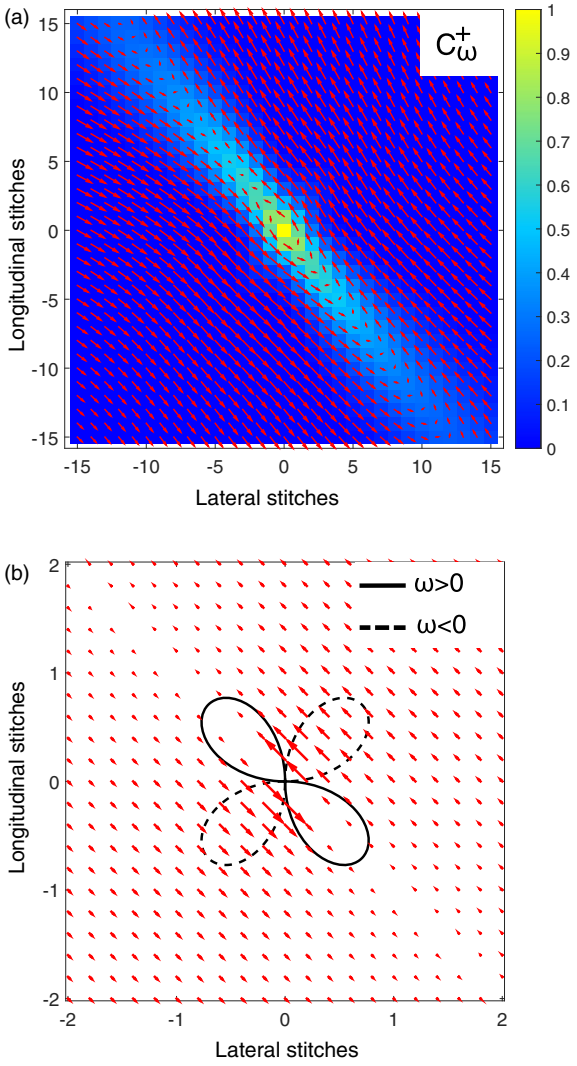

FIG. 4. Experimental spatial correlation and theoretical elastic deformation of positive events. (a) Amplitude of the correlation function C_{ω}^{+} of the vorticity, showing the events propagating along diagonal stitches, together with the relative displacement field during positive events $\vec{u}_{+}(\delta x,\delta y)=\langle\vec{u}(x+\delta x,y+\delta y)-\vec{u}(x,y)\rangle_{+}$. Data shown for $v=5$ μm/s. (b) Analytical response of the elastic network to a local perturbation shown through the displacement field around the perturbation, along with the angular dependence of the vorticity field $r^2\omega(r,\theta)$. The direction of maximum vorticity redistribution matches the orientation of the slip lines, suggesting that the events are formed by triggered successive slips.

Conclusion.—In this study, we show that the mechanical response of a knitted fabric displays crackling dynamics in its mechanical response through stick-slip events, despite its topologically protected structural order; thus, it is not prone to either structural rearrangement or yielding or failure. Global and local avalanche size display power law

distributions as those predicted by mean-field models of soft amorphous materials. This approach differs from previous studies on friction in textiles [33,34] and may trigger new perspectives for the study of textile mechanics. Moreover, the quality of the experimental measurements of the avalanche statistics in this original system ends up rivaling the latest similar experimental analysis on more commonly studied systems [3,6,22]. Knitted fabrics can thus be used as a tool to investigate the universal crackling response, allowing us to distinguish between the effects of plastic threshold distributions present here and the missing structural disorder. This approach also proves advantageous for several reasons such as a straightforward experimental implementation and analysis or the presence of numerous easily tunable parameters.

The authors thank E. Agoritsas, A. Rosso, and J.-L. Barrat for fruitful discussions. This work was carried out in the framework of the METAMAT Project No. ANR-14-CE07-0031 funded by Agence Nationale pour la Recherche.

*spoincloux@lps.ens.fr

[1] I. Albert, P. Tegzes, B. Kahng, R. Albert, J. G. Sample, M. Pfeifer, A.-L. Barabasi, T. Vicsek, and P. Schiffer, Phys. Rev. Lett. **84**, 5122 (2000).
[2] N. W. Hayman, L. Ducloué, K. L. Foco, and K. E. Daniels, Pure Appl. Geophys. **168**, 2239 (2011).
[3] D. Denisov, K. Lörincz, J. Uhl, K. Dahmen, and P. Schall, Nat. Commun. **7**, 10641 (2016).
[4] J. Lauridsen, M. Twardos, and M. Dennin, Phys. Rev. Lett. **89**, 098303 (2002).
[5] B. A. Sun, H. B. Yu, W. Jiao, H. Y. Bai, D. Q. Zhao, and W. H. Wang, Phys. Rev. Lett. **105**, 035501 (2010).
[6] J. Antonaglia, W. J. Wright, X. Gu, R. R. Byer, T. C. Hufnagel, M. LeBlanc, J. T. Uhl, and K. A. Dahmen, Phys. Rev. Lett. **112**, 155501 (2014).
[7] K. Chen, P. Bak, and S. P. Obukhov, Phys. Rev. A **43**, 625 (1991).
[8] D. Bonamy, S. Santucci, and L. Ponson, Phys. Rev. Lett. **101**, 045501 (2008).
[9] T. Chevalier, A. K. Dubey, S. Atis, A. Rosso, D. Salin, and L. Talon, Phys. Rev. E **95**, 042210 (2017).
[10] N. Friedman, A. T. Jennings, G. Tsekenis, J.-Y. Kim, M. Tao, J. T. Uhl, J. R. Greer, and K. A. Dahmen, Phys. Rev. Lett. **109**, 095507 (2012).
[11] G. Sparks and R. Maaß, Acta Mater. **152**, 86 (2018).
[12] L. Carrillo, L. Mañosa, J. Ortin, A. Planes, and E. Vives, Phys. Rev. Lett. **81**, 1889 (1998).
[13] J. T. Uhl *et al.*, Sci. Rep. **5**, 16493 (2015).
[14] E. Bouchbinder, J. S. Langer, and I. Procaccia, Phys. Rev. E **75**, 036107 (2007).
[15] K. A. Dahmen, Y. Ben-Zion, and J. T. Uhl, Nat. Phys. **7**, 554 (2011).
[16] J. Lin, E. Lerner, A. Rosso, and M. Wyart, Proc. Natl. Acad. Sci. U.S.A. **111**, 14382 (2014).
[17] See Supplemental Material at http://link.aps.org/supplemental/10.1103/PhysRevLett.121.058002 for further information on the experimental protocol, effects of different parameters, and calculation derivation.
[18] S. Papanikolaou, D. M. Dimiduk, W. Choi, J. P. Sethna, M. D. Uchic, C. F. Woodward, and S. Zapperi, Nature (London) **490**, 517 (2012).
[19] C. E. Maloney and M. O. Robbins, J. Phys. Condens. Matter **20**, 244128 (2008).
[20] C. Liu, E. E. Ferrero, F. Puosi, J.-L. Barrat, and K. Martens, Phys. Rev. Lett. **116**, 065501 (2016).
[21] A. Amon, V. B. Nguyen, A. Bruand, J. Crassous, and E. Clément, Phys. Rev. Lett. **108**, 135502 (2012).
[22] J. Barés, D. Wang, D. Wang, T. Bertrand, C. S. O'Hern, and R. P. Behringer, Phys. Rev. E **96**, 052902 (2017).
[23] A. Nicolas, E. E. Ferrero, K. Martens, and J.-L. Barrat, arXiv:1708.09194.
[24] J.-C. Baret, D. Vandembroucq, and S. Roux, Phys. Rev. Lett. **89**, 195506 (2002).
[25] E. Agoritsas, E. Bertin, K. Martens, and J.-L. Barrat, Eur. Phys. J. E **38**, 71 (2015).
[26] K. W. Desmond and E. R. Weeks, Phys. Rev. Lett. **115**, 098302 (2015).
[27] X. Cao, A. Nicolas, D. Trimcev, and A. Rosso, Soft Matter **14**, 3640 (2018).
[28] C. E. Maloney and A. Lemaitre, Phys. Rev. E **74**, 016118 (2006).
[29] A. Tanguy, F. Leonforte, and J.-L. Barrat, Eur. Phys. J. E **20**, 355 (2006).
[30] B. Tyukodi, S. Patinet, S. Roux, and D. Vandembroucq, Phys. Rev. E **93**, 063005 (2016).
[31] A. Le Bouil, A. Amon, S. McNamara, and J. Crassous, Phys. Rev. Lett. **112**, 246001 (2014).
[32] S. Poincloux, M. Adda-Bedia, and F. Lechenault, Phys. Rev. X **8**, 021075 (2018).
[33] M. Matsuo and T. Yamada, Text. Res. J. **79**, 275 (2009).
[34] G. Dusserre, Eur. J. Mech. A **51**, 160 (2015).